International Journal of Heat and Fluid Flow 29 (2008) 1190–1196

Contents lists available at ScienceDirect

International Journal of Heat and Fluid Flow

journal homepage: www.elsevier.com/locate/ijhff

Thermocapillary flows in liquid bridges of molten tin with small aspect ratios

K. Li [a], B. Xun [a], N. Imaishi [b,*], S. Yoda [c], W.R. Hu [a]

[a] Institute of Mechanics, Chinese Academy of Sciences, 15 Beisihuanxi Road, Beijing 100080, China
[b] Institute for Materials Chemistry and Engineering, Kyushu University, 6-1 Kasuga-koen, Kasuga 816-8580, Japan
[c] Japan Aerospace Exploration Agency, 2-1-1 Sengen, Tsukuba 305-0032, Japan

ARTICLE INFO

Article history:
Received 14 August 2007
Received in revised form 29 January 2008
Accepted 23 February 2008
Available online 7 April 2008

Keywords:
Oscillatory thermocapillary flow
Half-zone liquid bridge
Low-*Pr*-fluid
Molten tin
Numerical simulation

ABSTRACT

Numerical simulations were conducted to study thermocapillary flows in short half-zone liquid bridges of molten tin with Prandtl number $Pr = 0.009$, under ramped temperature difference. The spatio-temporal structures in the thermocapillary flows in short half-zone liquid bridges with aspect ratios $As = 0.6$, 0.8 and 1.0 were investigated. The first critical Marangoni numbers were compared with those predicted by linear stability analyses (LSA). The second critical Marangoni numbers for $As = 0.6$ and 0.8 were found to be larger than that for $As = 1.0$. The time evolutions of the thermocapillary flows exhibited unusual features such as a change in the azimuthal wave number during the three-dimensional stationary (non-oscillating) flow regime, a change in the oscillation mode during the three-dimensional oscillatory flow regime, and the decreasing and then increasing of amplitudes in a single oscillation mode. The effects of the ramping rate of the temperature difference on the flow modes and critical conditions were studied as well. In this paper, the experimental observability of the critical conditions was also discussed.

1. Introduction

Studies on the stability of thermocapillary flows in half-zone liquid bridges of fluids with low Prandtl number (*Pr*) are motivated by the experimentally proven fact that oscillatory thermocapillary flow in floating-zone configurations may be responsible for the striations in crystals grown in space (Croell et al., 1989). Since Rupp et al. (1989) first predicted the flow instability of the thermocapillary flow in a half-zone liquid bridge by numerical simulation, numerous linear stability analyses (LSA) and nonlinear direct numerical simulations (DNS) (e.g. see Kuhlmann, 1999; Davis and Smith, 2003; Lappa, 2005) have proved that the thermocapillary flows in nonisothermal half-zone liquid bridges and floating-zones of low-*Pr* fluids becomes oscillatory via a two-step bifurcation: the first bifurcation to a three-dimensional stationary flow occurs at a certain Marangoni number (the first critical Marangoni number Ma_{c1}) and the second bifurcation to a three-dimensional oscillatory flow occurs at a larger Marangoni number (the second critical Marangoni number Ma_{c2}). Very recently, nine research groups jointly performed a numerical benchmark work study (Shevtsova, 2005) on the first bifurcation of the thermocapillary flow in half-zone liquid bridges (hereafter, "half-zone" is eliminated) of low-*Pr* fluids. However, the results of the benchmark study on the second bifurcation to oscillatory thermocapillary flow were not available in the paper. In our previous numerical studies (Imaishi et al., 1999, 2000, 2001; Yasuhiro et al., 2000), the general features of the oscillatory thermocapillary flows in liquid bridges of low-*Pr* fluids ($Pr = 0.01$ and 0.02) under microgravity condition were systematically investigated for a wide range of aspect ratios (*As*) from 1.0 to 2.2, and the corresponding stability map was proposed (Imaishi et al., 2001). In the *As* range studied, the critical azimuthal wave number (m) of the three-dimensional stationary thermocapillary flow approximately agrees with the empirical correlation (Kuhlmann, 1999), namely, $m \approx 2/As$. For the oscillatory thermocapillary flow under slightly supercritical conditions, the flow and temperature field $F(\mathbf{x},\tau)$ can be expressed as the superposition of the time-dependent three-dimensional velocity or temperature disturbance $F'(\mathbf{x},\tau)$ and the time-averaged basic field $\overline{F}(\mathbf{x})$, i.e., $F(\mathbf{x},\tau) = \overline{F}(\mathbf{x}) + F'(\mathbf{x},\tau)$. Generally, the basic field inherits its characteristics from the corresponding three-dimensional stationary flow, however, the time-dependent velocity or temperature disturbance exhibits complex behavior. We reported three types of oscillation modes that were classified based on the time-dependent deformations of the flow and thermal fields in the mid-plane of the liquid bridges (Imaishi et al., 1999, 2000, 2001; Yasuhiro et al., 2000), the three types of oscillation modes were "*P*", "*T*" and "*R*", and they represent the "pulsating", "twisting", and "rotating" modes, respectively. The stability limits for the thermocapillary flows also exhibit a strong aspect-ratio (*As*) dependency as shown in Fig. 1. In the range of *As* studied, the Ma_{c2} profiles for liquid bridges of $Pr = 0.01$ and 0.009 show the maximum

* Corresponding author. Tel.: +81 92 583 7793; fax: +81 92 583 7796.
E-mail address: imaishi@cm.kyushu-u.ac.jp (N. Imaishi).

0142-727X/$ - see front matter © 2008 Elsevier Inc. All rights reserved.
doi:10.1016/j.ijheatfluidflow.2008.02.011

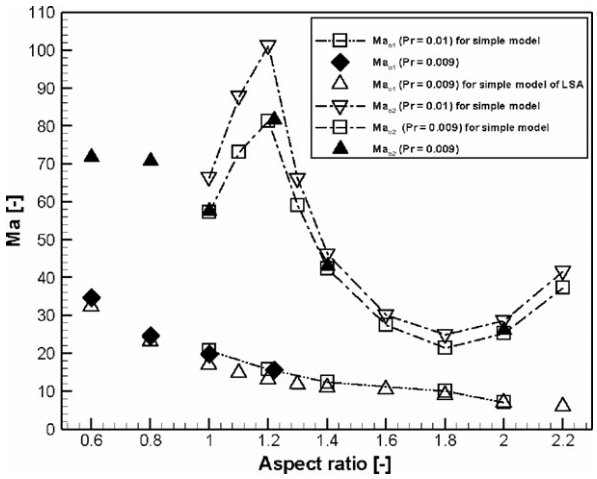

Fig. 1. Critical Marangoni number profiles as a function of aspect ratio.

values at around $As = 1.2$, and they decrease rapidly with the distance from $As = 1.2$. In most of the aforementioned numerical studies, a simple liquid bridge model in which the liquid bridge was supported between two isothermal discs with a constant temperature difference was adopted and the calculation domain was restricted to the melt zone.

Despite the large number of experimental studies (Han et al., 1996; Levenstam et al., 1996; Nakamura et al., 1998; Hibiya and Nakamura, 1999; Cheng and Kou, 2000; Sumiji et al., 2000, 2001, 2002; Azami et al., 2001a,b; Hibiya et al., 2001; Yang and Kou, 2001) on the oscillatory thermocapillary flow in the liquid bridges of low-*Pr* fluids, our understandings of this phenomena continue to remain insufficient due to the difficulties in conducting well-controlled experiments; these difficulties stem from the opacity, reactivity, and high melting point of low-*Pr* fluids (mostly liquid metals). Recently, JAXA (former NASDA) conducted a series of on-ground experimental studies (Takagi et al., 2001) on the liquid bridges of molten tin ($Pr = 0.009$) supported between iron rods. In these experimental studies, the free surface temperature oscillations were successfully observed by using radiation thermometers, however, the oscillations possess greater amplitudes and lower frequencies than those predicted by the numerical studies. For investigating the causes of these discrepancies, long-run numerical simulations were conducted based on realistic liquid bridge models of molten tin with $As = 1.22$ and 2.0 (Yasuhiro et al., 2004; Li et al., 2005) in which the heat transfer in the supporting iron rods was taken into account, further, in these simulations a ramped temperature difference was imposed to mimic the experimental condition. The numerical studies revealed that velocity oscillations with small amplitudes and high frequencies occur in the interior regions of the melt zone at the second bifurcation. However, free surface temperature oscillations can be detected much later due to the low *Pr* of molten tin. Thus, the value of Ma_{c2} determined by the experimentally observed free surface temperature oscillations may not correspond to the exact onset of the oscillatory flow. Despite these experimental difficulties, JAXA's experimental results for *As* larger than 1.2 appear to support the *As* dependency of Ma_{c2} predicted by our numerical simulations (Matsumoto et al., 2006). However, the decrease in *As* range from 1.2 to 1.0 has not been verified experimentally.

Despite the aforementioned experimental and numerical studies performed for studying the oscillatory thermocapillary flows in the liquid bridges of low-*Pr* fluids based on either the simple model or a realistic model, the number of investigations on the spatio-temporal details of three-dimensional thermocapillary flows for small aspect ratios (less than unity) is sparse. The objectives of this study are to extend the numerical studies to small aspect ratios and to explore the *As* dependency of the corresponding stability limits. Moreover, the effects of the ramping rate of the temperature difference on the flow modes and critical conditions are studied. Finally, a quantitative discussion on the experimental observability of the critical conditions is presented.

2. Problem statement

Fig. 2a shows the schematics of a more realistic liquid bridge model of molten tin considered in this study. The melt zone is assumed to be cylindrical and non-deformable under microgravity conditions. The molten tin is considered to be an incompressible Newtonian fluid with constant properties. A cylindrical coordinate system (r, θ, z) is adopted with the origin located at the center of the bottom of the melt zone. The radius of the liquid bridge is a, and the lengths of the melt zone and the iron rod are L and L_r, respectively. The corresponding *As* values of the melt zone and iron rods are given by $As = L/a$ and $As_r = L_r/a$, respectively. The fundamental equations are expressed in the dimensional form as follows:

In the liquid bridge,

$$\nabla \cdot \mathbf{U} = 0, \tag{2.1}$$

$$\frac{\partial \mathbf{U}}{\partial t} + \mathbf{U} \cdot \nabla \mathbf{U} = -\frac{1}{\rho}\nabla p + \nu \nabla^2 \mathbf{U}, \tag{2.2}$$

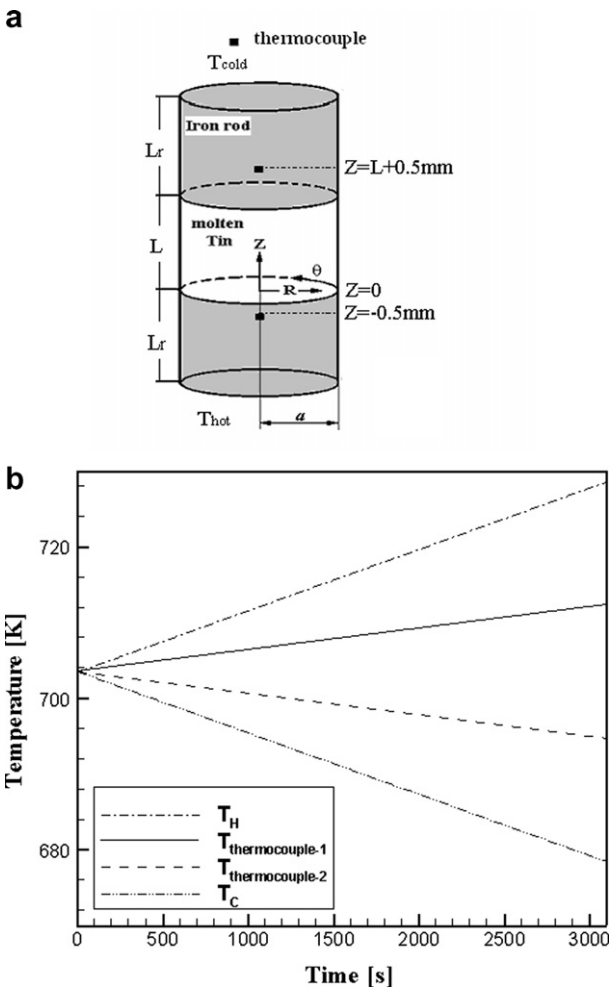

Fig. 2. Schematic of a realistic half-zone liquid bridge model (a), and the ramped temperature difference applied on the iron supporting rods (b).

$$\frac{\partial T}{\partial t} + \mathbf{U}\cdot\nabla T = \alpha\nabla^2 T. \tag{2.3}$$

In the iron rods,

$$\frac{\partial T}{\partial t} = \alpha_r \nabla^2 T. \tag{2.4}$$

Here, $\mathbf{U} = (U_r, U_\theta, U_z)$ is the velocity vector; ν, the kinetic viscosity; t, the time; ρ, the density; p, the pressure; T, the temperature; and α and α_r, the thermal diffusivities of the fluid and rods, respectively.

The boundary conditions are as follows:

On the melt surface ($r = a$),

$$U_r = 0, \quad \frac{\partial}{\partial r}\left(\frac{U_\theta}{r}\right) = -\frac{\sigma_T}{r^2\rho\nu}\frac{\partial T}{\partial\theta}, \quad \frac{\partial U_z}{\partial r} = -\frac{\sigma_T}{\rho\nu}\frac{\partial T}{\partial z}, \quad \frac{\partial T}{\partial r} = 0. \tag{2.5}$$

On the rod surface ($r = a$),

$$\frac{\partial T}{\partial r} = 0. \tag{2.6}$$

At the melt/rod interfaces ($z = L$ and $z = 0$),

$$U_r = U_\theta = U_z = 0, \quad k\frac{\partial T}{\partial z} = k_r\frac{\partial T}{\partial z}. \tag{2.7}$$

Here, k and k_r are the heat conductivities of the melt and rod, respectively.

It is supposed that at the initial time ($t = 0$), the molten tin was quiescent and at a uniform temperature of 703.6 K, and subsequently the time-dependent temperatures were imposed on each end of the iron rods (T_H and T_C) (see Fig. 2b). The ramping rate of the temperature difference, $d(T_H - T_C)/dt = 1.93$ K/min, was calculated based on the experimental value measured by thermocouples located at 0.5 mm apart from the melt/rod interfaces by means of a steady conduction model (Yasuhiro et al., 2004; Li et al., 2005). The Pr and Marangoni numbers in this study are defined as $Pr = \nu/\alpha$ and $Ma = -\frac{a\sigma_T\Delta T_e}{\rho\nu\alpha}$, respectively, where ΔT_e acting on the melt/solid interfaces is expressed as follows:

$$\Delta T_e = \left\{\int_0^{2\pi} T(a,\theta,0)d\theta - \int_0^{2\pi} T(a,\theta,L)d\theta\right\}/2\pi. \tag{2.8}$$

3. Numerical methods

3.1. Method for the non-linear numerical simulation

The fundamental equations are discretized through the control-volume finite difference method on staggered grids. Non-uniform grid distributions are adopted to increase the resolution near the boundaries. A full description of the numerical methods and the code validation can be found elsewhere (Yasuhiro et al., 2004). In this study, the total grid numbers are $40 \times 83 \times 96$ ($N_r \times N_\theta \times N_z$) (32 grids in the z-direction of the melt zone), $40 \times 83 \times 104$ (40 grids in the z-direction of the melt zone) and $40 \times 83 \times 104$ (40 grids in the z-direction of the melt zone) for cases with $As = 0.6$, 0.8 and 1.0, respectively. The numerical simulations were conducted on a Fujitsu VPP-5000 vector processor. The thermophysical properties and geometric parameters of the liquid bridge models are listed in Table 1.

3.2. Method for the linear stability analysis (LSA)

In the linear stability analysis, a basic steady axisymmetric state denoted by

$$\mathbf{X} = \{\mathbf{U}(r,z) = U_r\mathbf{e_r} + U_z\mathbf{e_z}, p(r,z), T(r,z)\}$$

is first determined for a given set of parameters (Ma, Pr and As), and subsequently small three-dimensional disturbances are added to the basic state and linearized by neglecting the high orders of disturbances. The disturbances are assumed to be in the normal mode

$$\begin{bmatrix}\mathbf{U}'(r,\ \theta,\ z,\ t,)\\ p'(r,\ \theta,\ z,\ t,)\\ T'(r,\ \theta,\ z,\ t,)\end{bmatrix} = \begin{bmatrix}\mathbf{U}'(r,\ z)\\ p'(r,\ z)\\ T'(r,\ z)\end{bmatrix}\exp(\gamma^{(m)}t + im\theta). \tag{3.1}$$

Here, the variables with the prime symbol indicate the disturbances: m, the azimuthal wave number: $\gamma^{(m)}$, the complex growth rate of the corresponding perturbation mode: and $i = \sqrt{-1}$. The discrete form of the linearized equations can be expressed as the generalized eigenvalue problem

$$\mathbf{g}(\mathbf{x},\mathbf{X},Ma,m,Pr,As) \equiv \mathbf{Ax} = \gamma\mathbf{Bx}, \tag{3.2}$$

where $\mathbf{x} \equiv (U_r, U_\theta, U_z, p, T)^{\mathbf{T}}$ denotes a vector comprising the disturbance velocity, pressure and temperature. $\mathbf{A}$ is a real-valued non-symmetric matrix, while $\mathbf{B}$ is a singular real-valued diagonal matrix. The eigenvalues and related eigenfunctions of problem (3.2) are solved for a given set of parameters. For each value of m, the Marangoni number corresponding to the marginal stability limit (the real part of $\gamma^{(m)}$ is zero) is determined. Ma_{c1} is obtained as the minimum value among all the m values. The numerical method and its validations are reported in detail elsewhere (Xun et al., in press). It must be noted that the LSA was conducted on simple liquid bridge models with constant (uniform and time-independent) temperature differences.

Table 1
Thermophysical properties and geometric parameters

	Molten tin	Iron
Pr	0.009	–
Density ρ (kg/m^3)	6793	7700
Thermal conductivity k (W/mK)	35.44	20.0
Specific heat C_p (J/kg K)	242	460
Viscosity μ (kg/ms)	1.318×10^{-3}	–
Temperature gradient of surface tension σ_T (N/mK)	-1.3×10^{-4}	–
Radius a (m)	3.0×10^{-3}	
Offset of the thermocouple junction from melt/rod interface δ (m)	0.5×10^{-3}	

4. Numerical results

In order to explore the spatio-temporal details of the thermocapillary flows in liquid bridges of molten tin with small As and to implement the corresponding stability boundaries, numerical simulations were conducted based on realistic liquid bridge models with $As = 0.6$, 0.8 and 1.0. The computed results are compared with the LSA results in the following sections.

4.1. Liquid bridge of molten tin with As = 0.6

Before the first bifurcation, the thermocapillary flow is axisymmetric and non-oscillatory. At $t = 900.0$ s, and $\Delta T_e = 2.53$ K, the azimuthal velocities on the free surface become non-zero and grow rapidly, indicating the formation of a three-dimensional flow field. Thus, Ma_{c1} is determined to be 34.73. The free surface temperatures also deviate from the uniform and monotonic increase with time, which reflects the axisymmetric stationary flow field existing at that instant (details will be discussed in Section 5). Fig. 3 indicates that the developed three-dimensional flow field is characterized by an azimuthal wave number of $m = 3$. Table 2 shows Ma_{c1} values and the corresponding critical azimuthal wave numbers based on the LSA for $Pr = 0.009$. It can be observed that the Ma_{c1} value determined through the present numerical simulations is close to the LSA result for $As = 0.6$ ($Ma_{c1} = 32.31$). With a further increase

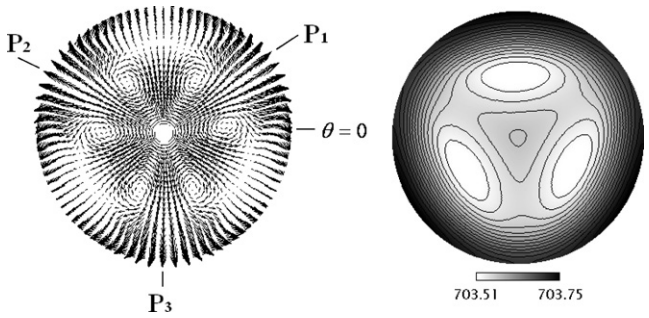

Fig. 3. Velocity and temperature distributions on the mid-plane ($z = 0.5L$) for stationary three-dimensional flow in liquid bridge of $As = 0.6$: $m = 3$ at $Ma = 42.44$.

Table 2
LSA results for the first bifurcation

As	Ma_{c1}	m
0.6	32.31	3
0.8	23.18	2
1.0	17.00	2
1.1	14.81	2
1.2	13.06	2
1.3	11.80	2
1.4	11.00	2
1.6	10.42	2
1.8	8.89	1
2.0	6.94	1
2.2	5.92	1

in the temperature difference, the three-dimensional velocity and temperature fields gradually evolve into the saturated regime. The 3D flow field becomes unstable and changes to an oscillatory flow. In this study, as an indicator for the second bifurcation, the maximum absolute value of the radial velocity near the axis $|U_r(r \to 0, z = 0.5L)|_{max}$ was chosen due to its sensitivity to the incipience of oscillatory flow (Li et al., 2005). Fig. 4 shows the time evolutions of the indicator velocity and the free surface temperature at the center ($z = 0.5L$) of the liquid bridge. The flow begins to exhibit oscillations with a frequency of 0.128 Hz (determined through FFT)

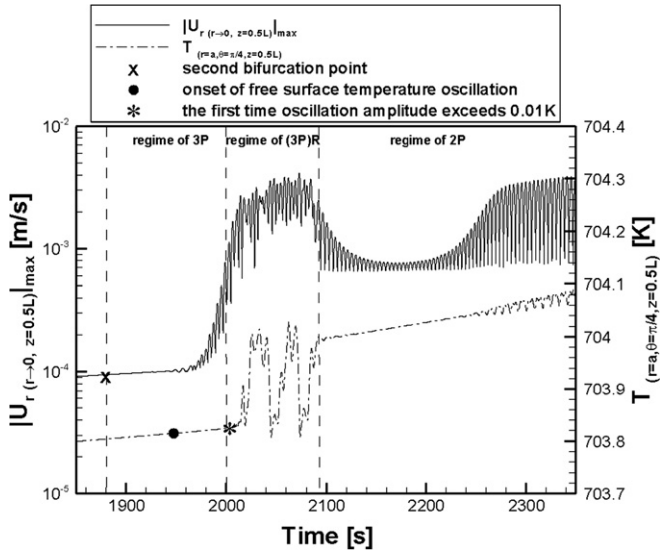

Fig. 4. Time evolutions of indicator velocity and a free surface temperature at $z = 0.5L$ for liquid bridge with $As = 0.6$.

at $t = 1880.0$ s, $\Delta T_e = 5.24$ K, and $Ma_{c2} = 71.93$. However, the thermal field does not respond quickly to the flow oscillations that start near the axis. The free surface temperature generates oscillations at $Ma = 74.47$ (normalized distance from the second bifurcation: $\varepsilon_2 = (Ma - Ma_{c2})/Ma_{c2} = 0.035$). A similar phenomenon was observed in the case of $As = 1.22$ (Li et al., 2005). During the process of development of the oscillatory flow, different wave numbers and oscillation modes were observed as shown in Fig. 4. At slightly super critical conditions (immediately after the second bifurcation point), the basic flow field of $m = 3$ is modulated by a periodic pendulum-like pulsating motion: this pulsating motion first induces a radial velocity across the axis back and forth along P_1 (see Fig. 3), which is followed by a similar pulsating motion along P_2, and then along P_3. The type of oscillation mode is denoted as 3*P*. These asymmetric pulsating actions stimulate the azimuthal velocity field. At approximately $t = 2000$ s, the entire velocity and temperature fields exhibiting 3*P* oscillation start bulk rotation around the *z*-axis. Let us denote this type of oscillation mode as (3*P*)*R*. The surface temperature during the (3*P*)*R* oscillation exhibits two characteristic frequencies of 0.13 Hz (corresponding to the 3*P* oscillations) and 0.021 Hz (corresponding to the bulk rotation with a period of 142.9 s.). When the temperature difference increased further, $\Delta T_e = 5.82$ K and $Ma = 79.93$ ($\varepsilon_2 = 0.11$) at $t = 2092.0$ s, and the type of oscillation mode showed a quick transition to 2*P* (it was also expressed as (2 + 1) in our previous reports (Imaishi et al., 1999, 2000, 2001; Yasuhiro et al., 2000)): the rotation stopped and this was accompanied by a decrease in the oscillation amplitudes. However, after $t = 2177.0$ s, $\Delta T_e = 6.05$ K and $Ma = 83.12$ ($\varepsilon_2 = 0.16$), the oscillation amplitudes of the 2*P* type oscillation mode increase quickly and reached the saturated regime in which the oscillation amplitudes continued increasing gradually until the end of the present simulation ($t = 2550.1$ s, $\Delta T_e = 7.06$ K, $Ma = 96.92$ and $\varepsilon_2 = 0.35$). The transition of the oscillation modes from 3*P* through (3*P*)*R* to 2*P* suggests that the basic mode of $m = 2$ is more favorable (or stable) in the moderately supercritical region than that of $m = 3$.

4.2. Liquid bridge of molten tin with As = 0.8

In this case, the axisymmetric thermocapillary flow breaks up into a three-dimensional stationary flow of $m = 2$ (see Fig. 5a) at the first bifurcation point ($t = 560.4$ s, $\Delta T_e = 1.80$ K and $Ma_{c1} = 24.71$), as shown in Fig. 6. Thus, the Ma_{c1} value that is determined is consistent with the LSA result shown in Table 2 ($Ma_{c1} = 23.18$). However, this stationary three-dimensional flow becomes unstable at a larger temperature difference. At $t = 1181.3$ s, $\Delta T_e = 3.75$ K and $Ma = 51.48$, the velocity and temperature fields deform the patterns along the shorter axis (P_s) of the $m = 2$ velocity field (Imaishi et al., 1999). The resultant three-dimensional stationary fields resemble that of a mixture of velocity and temperature fields of $m = 2$ and $m = 3$, as shown in Fig. 5b. Such a two-step bifurcation of the non-oscillating thermocapillary flow (see Fig. 6) has never been observed in our numerical simulations with ramped temperature difference (Yasuhiro et al., 2004; Li et al., 2005). Oscillations in the flow field starts at $t = 1640.1$ s, $\Delta T_e = 5.16$ K and $Ma_{c2} = 70.84$ at the critical frequency of 0.067 Hz. The oscillatory disturbance exhibits a periodic pendulum-like pulsating motion that induces a radial velocity across the axis back and forth along P_s (Imaishi et al., 1999). It must be noted that a considerably long time gap is needed before large amplitude oscillations occurs, and the oscillation amplitudes decrease instantly (see Fig. 7). However, at $t = 1875.0$ s, $\Delta T_e = 5.87$ K and $Ma = 80.59$ ($\varepsilon_2 = 0.14$), the oscillatory flow is developed again and the amplitude increases steadily until the end of the present simulation ($t = 2069.9$ s, $\Delta T_e = 6.45$ K, $Ma = 88.51$ and $\varepsilon_2 = 0.25$). In this case, the free surface temperatures start oscillations at $Ma = 74.27$, and the lag between the on-

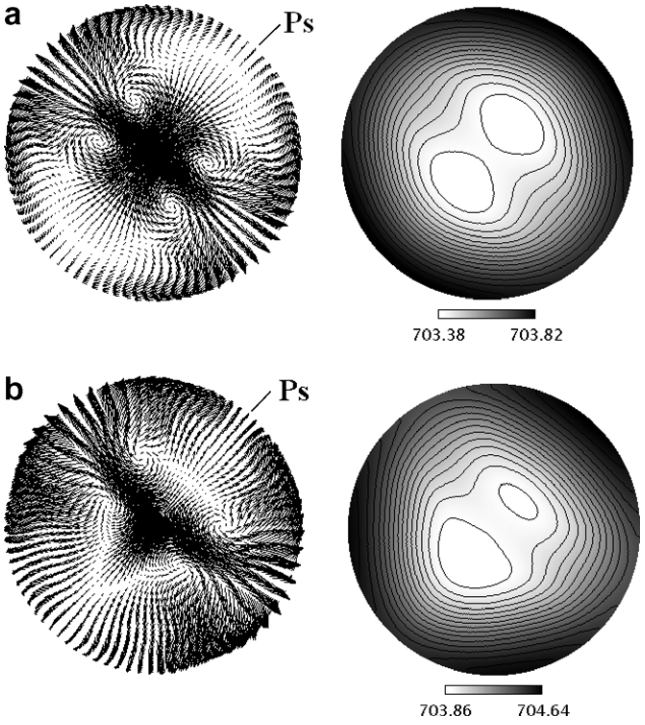

Fig. 5. Stationary three-dimensional flow in liquid bridge of $As = 0.8$. (a) Velocity and temperature distributions on $z = 0.5L$ observed at $Ma = 44.90$ ($m = 2$). (b) Velocity and temperature distributions on $z = 0.5L$ observed at $Ma = 60.03$ (mixture of $m = 2$ and $m = 3$). Temperature distributions are expressed by the gray scale.

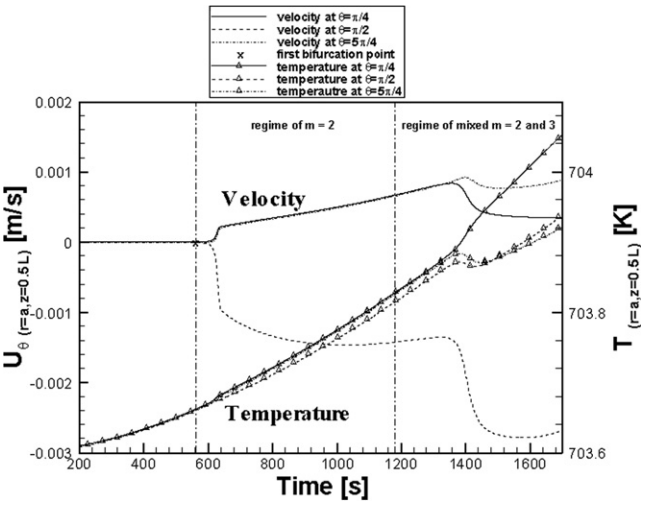

Fig. 6. Time evolutions of three-dimensional stationary flow in liquid bridge of $As = 0.8$. Azimuthal velocities and temperatures observed at three different points at $z = 0.5\ L$ are plotted as a function of time.

sets of the velocity and the free surface temperature oscillations is $\varepsilon_2 = 0.048$.

4.3. Liquid bridge of molten tin with As = 1.0

Since the numerical simulation results for the case of $As = 1.0$ are very similar to those of the simple liquid bridge model for $Pr = 0.01$ (Kuhlmann, 1999), we describe only them briefly as follows. The mode of the three-dimensional stationary flow is $m = 2$ after the first critical condition is established at $Ma_{c1} = 19.77$. The second bifurcation occurs at $Ma_{c2} = 57.66$, and the three-dimensional oscillatory flow is of the typical $2P$ type (Imaishi et al., 1999) with a critical frequency of 0.257 Hz. The free surface temperatures starts oscillations at $Ma = 59.20$, and the lag between the onsets of the velocity and the free surface temperature oscillations is $\varepsilon_2 = 0.027$. The oscillatory thermocapillary flow of the $2P$ type remains until the end of the present simulation ($\Delta T_e = 4.64$ K, $Ma = 63.76$ and $\varepsilon_2 = 0.11$).

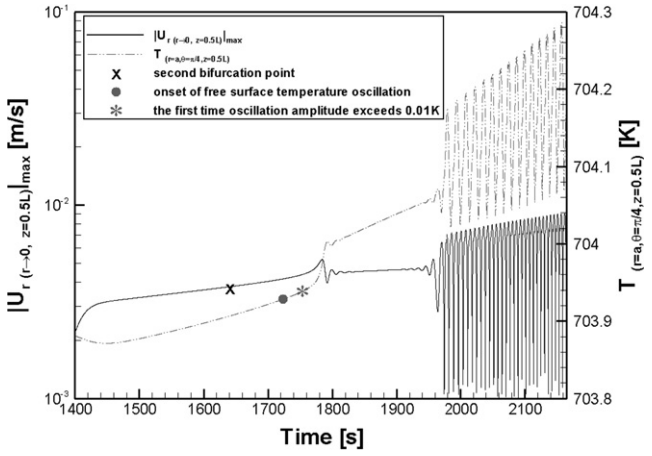

Fig. 7. Time evolution of three-dimensional oscillatory flow in liquid bridge of $As = 0.8$, expressed by the indicator velocity ($|U_r\ (0, \theta, 0.5\ L)|_{max}$) and a free surface temperature at $(a, \pi/4, 0.5L)$ as a function of time.

4.4. Stability boundaries for liquid bridges of molten tin

Fig. 1 summarizes the stability limits for the liquid bridges of molten tin ($Pr = 0.009$ and 0.01). In the As range studied so far, the Ma_{c1} determined by direct numerical simulations based on the more realistic liquid bridge model with a ramping rate of $(d(T_H - T_C)/dt = 1.93$ K/min) agrees fairly well with the LSA results based on the simple liquid bridge model. The Ma_{c1} profile decreases monotonously with an increasing As value up to 1.8, and this is followed by a gradual increase again. In the As range from 1.2 to 1.0, the numerical results based on the models exhibit a decrease in Ma_{c2} for both the Pr values. However, for smaller As values (less than unity), Ma_{c2} increases again and then becomes almost constant as As decreases below 0.8. It must be noted that in the As range studied, the pulse-like three-dimensional oscillatory disturbance prevails at the onset of the second bifurcation. The agreement between the critical Marangoni numbers obtained by numerical simulations based on both the simple and the realistic models with a small temperature ramping rate suggests that the heat conduction in the supporting rods and the method of application of the temperature difference do not significantly affect the stability of the thermocapillary flow.

In order to evaluate the effects of the ramping rate of the temperature difference on the stability limits, numerical studies based on realistic liquid bridge models with $As = 0.6$ and 0.8 and a larger ramping rate of $d(T_H - T_C)/dt = 11.57$ K/min (approximately six times that of the aforementioned ramping rate) were conducted. The computed results are tabulated in Table 3 together with the previous result for $As = 1.22$ (Li et al., 2005). For all the cases, the flow transition requires a large ΔT_e for a large temperature ramping rate. However, the differences are rather small for a liquid bridge with $As = 0.8$. Fig. 8 provides an explanation for this; for example, oscillations under larger temperature ramp rates begin without the saturated regime of the 3D stationary flow (mixture of $m = 2$ and $m = 3$). Therefore, the faster ramping rate tends to stabilize the stationary thermocapillary flow and also affects the time evolution of the flow to a certain extent.

Table 3
Effects of the temperature ramping rate on Ma_{c1} and Ma_{c2}

$d(T_H-T_C)/dt$ (K/min)	As = 0.6		As = 0.8		As = 1.22	
	Ma_{c1}	Ma_{c2}	Ma_{c1}	Ma_{c2}	Ma_{c1}	Ma_{c2}
1.93	34.73	71.93	23.18	70.84	15.68	81.7
11.57	36.65	75.50	27.45	71.38	20.19	84.4

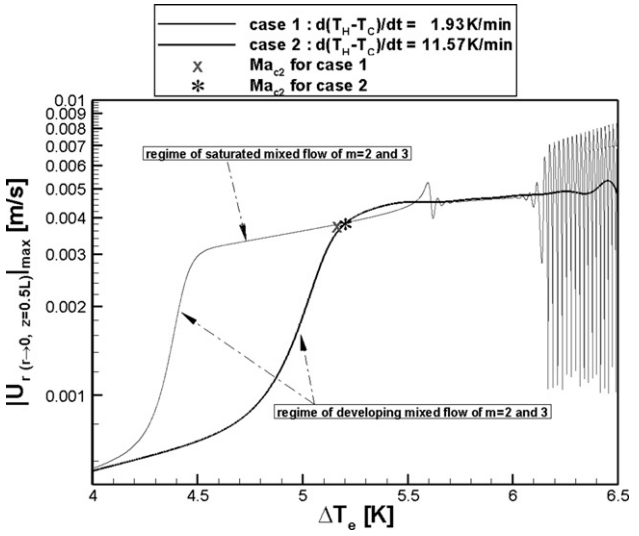

Fig. 8. Effect of ramping rate of temperature difference on the time evolution of 3D flows in a liquid bridge with $As = 0.8$. Ramping rates: $d(T_H - T_C)/dt = 1.97$ K/min and $d(T_H - T_C)/dt = 11.57$ K/min.

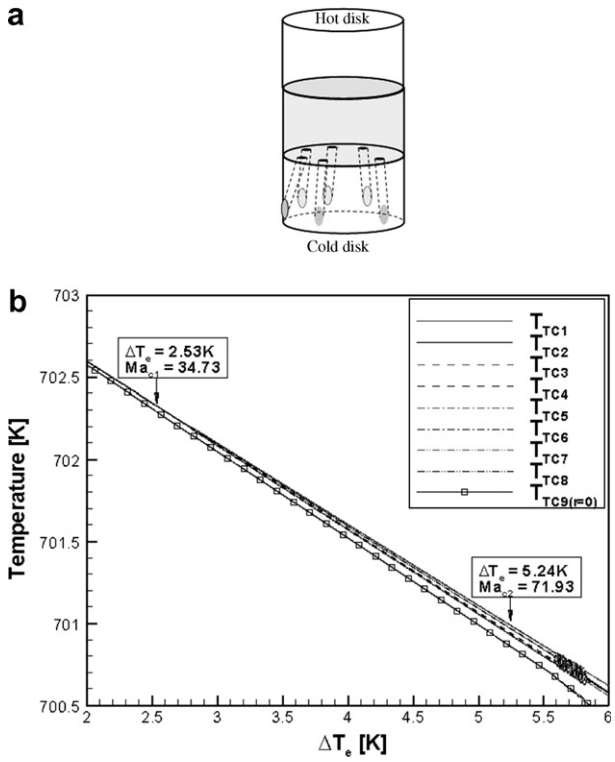

Fig. 9. Thermocouple positions and calculated temperature changes. (a) Thermocouples embedded in the cold rod in the experimental apparatus. (b) The numerical temperature recordings at the monitoring points on the cold rod/melt interface for $As = 0.6$.

5. Discussion on the experimental observability

Recently, JAXA has been attempting to detect the critical conditions for flow transitions in the liquid bridges of molten tin and to obtain a detailed information of the flow modes (Matsumoto et al., 2006) through temperature measurements by employing 8 or 9 thermocouples embedded in the cold rod (see Fig. 9a). Fig. 9b shows the temperature records obtained in the present simulation on the cold rod/melt interface for the case with $As = 0.6$. The locations of the monitoring points coincide with the TC positions, as shown in the inset. The temperature records reveal that the temperature at the center of the cold melt/rod interface is always colder than that near the periphery. Thus, the isothermal boundary condition adopted for the simple model does not prove to be useful and there always exists a 2D temperature distribution at the melt/rod interface. It also shows that the temperatures TC1–TC8 (located on a circle) remain exactly the same up to the first critical point ($\Delta T_{ec1} = 2.53$ K), reflecting the axisymmetric flow and temperature fields. However, these temperatures deviate from each

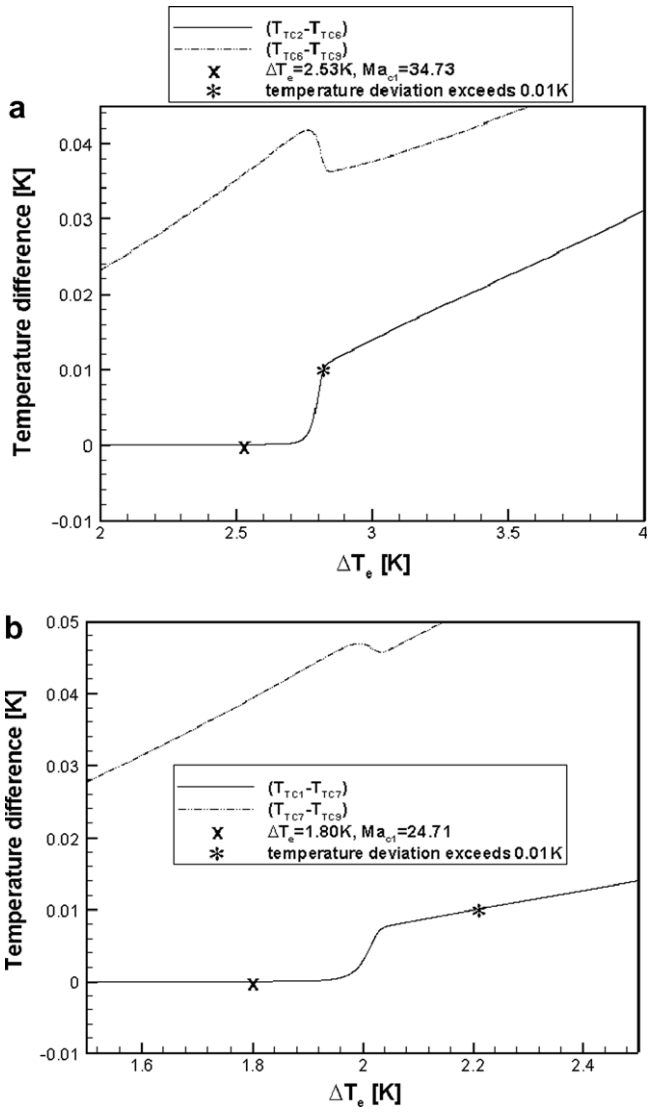

Fig. 10. Numerical results of the maximum temperature difference among the eight monitoring points (from TC1 to TC8) on the rod/melt interface. For $As = 0.6$. At the bifurcation point indicated by symbols $*$, $Ma = 38.4$ ($\Delta T_e = 2.82$ K). (b) For $As = 0.8$. At the bifurcation point indicated by symbols $*$, $Ma = 30.28$ ($\Delta T_e = 2.21$ K).

other after the first critical condition and start oscillations after the second critical condition ($\Delta Te_{c2} = 5.24$ K). Fig. 10 shows the plots of the maximum temperature differences among the eight monitoring points (from TC1 to TC8) together with the maximum temperature difference from TC9 (located at the center of the disk). By assuming the sensitivity of the temperature measurement system to be 0.01 K, the first bifurcation point can be detected at $Ma = 38.74$ (indicated by a symbol $*$ in Fig. 10a) and the second bifurcation at $Ma = 76.56$ (symbol $*$ in Fig. 4). These bifurcation points cause relative errors such as $\varepsilon_{c1} = (Ma - Ma_{c1})/Ma_{c1} = 0.115$ and $\varepsilon_{c2} = 0.064$. Fig. 10b indicates that the experimentally detectable first bifurcation condition for the case with $As = 0.8$ becomes $Ma = 30.28$ ($*$ in Fig. 10b) with a relative error of $\varepsilon_{c1} = 0.225$, and the second bifurcations should occur at $Ma = 75.50$ ($\varepsilon_{c2} = 0.066$) ($*$ in Fig. 7). These results reveal that there is no way to avoid errors in the detection of flow transitions through temperature measurements because of the time lags between the flow transitions and the temperature changes. There are two types of time lags: the first type is the lag between the changes in the velocity field and temperature field, and the second type is the lag induced by the sensitivity of the temperature measurement system. Improving the temperature measurement sensitivity reduces the second type of lag, however, the first type of lag is intrinsic for the liquid bridges of low-*Pr* fluids and independent of the sensitivity of the temperature measurement system. Thus, an accurate and sensitive velocity measurement system is required for the accurate experimental determination of Ma_{c1} and Ma_{c2} in liquid bridges of low-*Pr* fluids.

6. Conclusion

In this study, numerical simulations were conducted on the Marangoni convection in half-zone liquid bridges of molten tin with $As = 0.6$, 0.8, and 1.0 by using a realistic models of a liquid bridge in which the supporting iron rods and ramped temperature difference are taken into account. The critical condition for the first flow transition determined by the present simulation with a low ramping rate (1.93 K/min) approached the critical conditions determined by the simple model as well as LSA. Ma_{c1} increases monotonously with a decrease in the *As* for a wide range of *As* values between 0.6 and 2.2. Further, the Ma_{c2} values are also found to be close to those in our previous results of the simple model when the incipience of oscillations is monitored by observing the radial velocity on the center line. The oscillating flow starts in the pulsating mode in the liquid bridges with $As = 0.6$, 0.8, and 1.0. However, Ma_{c2} exhibits a relatively complicated *As* dependency, i.e., it shows a steep decrease with *As* from 1.2 to 1.0, and this is followed by an increase in the *As* range between 1.0 and 0.8, subsequently, Ma_{c2} becomes almost constant until $As = 0.6$. Two unusual phenomena were observed in the present simulations: the first one is the change in the azimuthal wave number during the three-dimensional non-oscillatory flow regime in the case of $As = 0.8$, and the second is a change in the azimuthal wave number during the oscillatory flow regime in the case of $As = 0.6$. Moreover, the pulse-like three-dimensional oscillatory disturbance prevails at the onset of the second bifurcation. The effects of the ramping rate of the temperature difference on the flow modes and critical conditions were studied. The computed results revealed that a large ramping rate tends to result in larger values for the critical Marangoni number. Finally, a quantitative discussion on the experimental observability of the critical conditions was presented. The results revealed that apart from temperature measurements, an accurate and sensitive measurement system is strongly required for the accurate experimental determination of Ma_{c1} and Ma_{c2} in the liquid bridges of low-*Pr* fluids.

References

Azami, T., Nakamura, S., Hibiya, T., Nakamura, S., 2001a. The effect of oxygen on the temperature fluctuation of Marangoni convection in a molten silicon bridge. Journal of Crystal Growth 223, 116–124.

Azami, T., Nakamura, S., Hibiya, T., 2001b. Observation of periodic thermocapillary flow in a molten silicon bridge by using non-contact temperature measurements. Journal of Crystal Growth 231, 82–88.

Cheng, M., Kou, S., 2000. Detecting temperature oscillation in a silicon liquid bridge. Journal of Crystal Growth 218, 132–135.

Croell, A., Mueller-Sebert, W., Nitsche, R., 1989. The critical Marangoni number for the onset of time-dependent convection in silicon. Materials Research Bulletin 24, 995–1004.

Davis, D.A.R., Smith, F.T., 2003. Flow and thermal convection in full-zone liquid bridges of wide-ranging aspect ratio. Theoretical and Computational Fluid Dynamics 17, 113–146.

Han, J.H., Sun, Z.W., Dai, L.R., Xie, J.C., Hu, W.R., 1996. Experiment on the thermocapillary convection of a mercury liquid bridge in a floating half-zone. Journal of Crystal Growth 169, 129–135.

Hibiya, T., Nakamura, S., 1999. Fluid flow in silicon melt with free surface, gravitational effects in materials and fluid sciences. Advances in Space Research 24, 1225–1230.

Hibiya, T., Nakamura, S., Azami, T., Sumiji, M., Imaishi, N., Mukai, K., Onuma, K., Yoda, S., 2001. Marangoni flow of molten silicon. Acta Astronautica 48, 71–78.

Imaishi, N., Yasuhiro, S., Sato, T., Yoda, S., 1999. Three dimensional numerical simulation of oscillatory Marangoni flow in half-zone of low-*Pr* fluids. In: Proceedings of Material Research in Low Gravity II, SPIE International Symposium on Optical Science, Engineering and Instrumentation, vol. 3792. pp. 344–352.

Imaishi, N., Yasuhiro, S., Sato, T., Yoda, S., 2000. Numerical simulation of three dimensional oscillatory flow in half-zone bridges of low *Pr* fluid. In: Proceedings of the 4th JSME–KSME Thermal Engineering Conference. pp. 277–282.

Imaishi, N., Yasuhiro, S., Akiyama, Y., Yoda, S., 2001. Numerical simulation of oscillatory Marangoni flow in half-zone liquid bridge of low Prandtl number. Journal of Crystal Growth 230, 164–171.

Kuhlmann, H.C., 1999. Thermocapillary Convection in Models of Crystal Growth. Springer, New York.

Lappa, M., 2005. Analysis of flow instabilities in convex and concave floating zones heated by an equatorial ring under microgravity conditions. Computers & Fluids 34, 643–770.

Levenstam, M., Amberg, G., Carlberg, T., Andersson, M., 1996. Experimental and numerical studies of thermocapillary convection in a floating zone like configuration. Journal of Crystal Growth 158, 224–230.

Li, K., Yasuhiro, S., Imaishi, N., Yoda, S., 2005. Marangoni flow in half-zone liquid bridge of molten tin under ramped temperature difference. Journal of Crystal Growth 280, 620–631.

Matsumoto, S., Ohira, H., Mashiko, T., Sasaki, H., Yoda, E., Imaishi, N., Yoda, S., 2006. Thermocapillary flow in low *Pr* number liquid bridge – Annual report of fluid dynamics instability research-, JAXA Research and Development Report, JAXA-RR-05-023E: <http://stage.tksc.jaxa.jp/library/report/search-17/list/list-syu.htm#RR>.

Nakamura, S., Hibiya, T., Kakimoto, K., Imaishi, N., Nishizawa, S., Hirata, A., Mukai, K., Yoda, S., Morita, T.S., 1998. Temperature fluctuations of the Marangoni flow in a liquid bridge of molten silicon under microgravity on board the TR-IA-4 rocket. Journal of Crystal Growth 186, 85–94.

Rupp, R., Mueller, G., Neumann, G., 1989. Three-dimensional time-dependent modeling of the Marangoni convection in zone-melting configurations for GaAs. Journal of Crystal Growth 97, 34–41.

Shevtsova, V.J., 2005. Thermal convection in liquid bridges with curved free surface: Benchmark of numerical solutions. Journal of Crystal Growth 280, 632–651.

Sumiji, M., Nakamura, S., Onuma, K., Hibiya, T., 2000. optical measurement of resonant oscillation and Marangoni convection-induced oscillation in a molten silicon surface. Japanese Journal of Applied Physics 39 (Part 1), 3688–3693.

Sumiji, M., Nakamura, S., Azami, T., Hibiya, T., 2001. Optical observation of solid-melt interface fluctuation due to Marangoni flow in a silicon liquid bridge. Journal of Crystal Growth 223, 503–511.

Sumiji, M., Nakamura, S., Hibiya, T., 2002. Two-directional observation of solid-melt interface fluctuation induced by Marangoni flow in a silicon liquid bridge. Journal of Crystal Growth 235, 55–59.

Takagi, K., Ohtaka, M., Natsui, H., Arai, T., Yoda, S., Yuan, Z., Mukai, K., Yasuhiro, S., Imaishi, N., 2001. Experimental study on transition to oscillatory thermocapillary flow in a low Prandtl number liquid bridge. Journal of Crystal Growth 233, 399–407.

Xun, B., Chen, G.C., Li, K., Yin, Z.H., Hu, W.R., in press. A linear stability analysis of large-Prandtl-number thermocapillary liquid bridges. Advances in Space Research.

Yang, Y.K., Kou, S., 2001. Temperature oscillation in a tin liquid bridge and critical Marangoni number dependency on Prandtl number. Journal of Crystal Growth 222, 135–143.

Yasuhiro, S., Sato, T., Imaishi, N., Yoda, S., 2000. Three dimensional Marangoni flow in liquid bridge of low *Pr* fluid. Space Forum 6, 39–48.

Yasuhiro, S., Li, K., Imaishi, N., Akiyama, Y., Natsui, H., Matsumoto, S., Yoda, S., 2004. Oscillatory Marangoni flow in half-zone liquid bridge of molten tin. Journal of Crystal Growth 266, 152–159.